Electrochemical Behavior of Morphology-Controlled Copper (II) Hydroxide Nitrate Nanostructures

Julien Sarmet, Christine Taviot-Gueho, Rodolphe Thirouard, Fabrice Leroux, Camille Douard, Insaf Gaalich, Thierry Brousse, Gwenaëlle Toussaint, Philippe Stevens

Electrochemical behavior of morphology controlled copper(II) hydroxide nitrate nanostructures.

Julien Sarmet, Christine Taviot-Gueho,* Rodolphe Thirouard, Fabrice Leroux, Camille Douard, Insaf Gaalich, Thierry Brousse, Gwenaëlle Toussaint and Philippe Stevens

Université Clermont Auvergne, Clermont Auvergne INP, CNRS, Institut de Chimie de Clermont Ferrand, F-63000 Clermont–Ferrand, France.

ABSTRACT: Nanostructure control is an important issue when using electroactive materials in energy conversion and storage devices. In this study, we report various methods of synthesis of nanostructured copper(II) hydroxide nitrate $Cu_2(OH)_3NO_3$ with layered hydroxide salt (LHS) structure using various synthesis methods and investigate the correlation between nanostructure, morphology and their pseudocapacitive electrochemical behavior. The variations in nanostructure size and morphology were comprehensively explored by combining X-ray diffraction (XRD)and scanning electron microscopy (SEM) whilst the electrochemical activity was characterized using cyclic voltammetry. We demonstrate that $Cu_2(OH)_3NO_3$ - LHS nanostructured submicron particles produced by alkaline precipitation with 88% of the copper cations can cycle with a two-electron redox process. Unfortunately, the electroactivity decreases rapidly from the first cycle due to the occurrence of structural transformations and subsequent electrochemical grinding. However, samples obtained by ultra-sonication and microwave synthesis, two original synthesis methods for LHS materials, formed of nanosized crystalline domains agglomerated in micron-sized particles, represent a good compromise between capacity and cyclability. Moreover, by using pair distribution function analysis on electrode materials after repeated cycling, we were able to follow the chemical and structural changes occurring in $Cu_2(OH)_3NO_3$ materials during electrochemical cycling with first a quick transformation to Cu_2O and then the appearance of Cu metal and copper acetate $Cu(II)_2(O_2CCH_3)_4.2H_2O$.

INTRODUCTION

The transformation of the energy system to a world without fossil fuels is a strong driving force to develop effective electrochemical energy conversion and storage devices based on batteries, fuel cells, and super capacitors. Efforts must focus on the development of inexpensive electrode materials with high redox reversibility and stability and in this field, layered hydroxide salts (LHS), also known as layered basic salts, benefit from a growing interest. Their structure is based on a distorted Brucite-like structure in which a fraction of the structural hydroxide groups is replaced by water molecules or anions leading to the following general chemical formula $M^{2+}(OH)_2{}^{x-}(A^{m-})_{x/m}\cdot nH_2O$, where M^{2+} is a divalent cation, normally Mg^{2+}, Ni^{2+}, Zn^{2+}, Ca^{2+}, Cd^{2+}, Co^{2+} or Cu^{2+}, and $(A^{m-})_{x/m}\cdot nH_2O$ is a counter-ion which is hydrated or not.[1] So far, the main focus has been on nickel- and cobalt-based LHS materials and promising electrochemical,[2, 3] magnetic,[4] and photophysical properties[5] have been reported. Layered copper hydroxide salts have been comparatively less studied although copper(II) hydroxide nitrate $Cu_2(OH)_3NO_3$ is used in vehicle airbags,[6] as well as a precursor[7] in the preparation of CuO p-type semiconductor for diverse applications in heterogeneous catalysis,[8] gas sensors,[9, 10] field emission semiconductors, lithium ion batteries,[11, 12] and high power aqueous batteries.[13, 14, 15, 16] These few studies clearly show the potential of layered copper hydroxide salts but also the need to better document and understand the synthesis of these materials to improve their performances.

In this study, by using similar synthesis protocol as reported for layered zinc hydroxide salts (LZH), but also new synthesis routes based on sonochemistry (US) and microwave (MW), we report the formation of well-defined nanostructured $Cu_2(OH)_3NO_3$ with various morphologies and sizes. First, microcrystalline parameters and morphological structures were comprehensively explored by combining scanning electron microscopy (SEM) and X-ray diffraction (XRD). In a second part, the electrochemical properties were investigated by cyclic voltammetry and pair distribution function (PDF) analyses were performed to examine phase transformations during cycling.

Table 1. Synthesis conditions and characteristics of $Cu_2(OH)_3NO_3$ sample series.

			Synthetic conditions						LHS characteristics		
Method Code	Salt	Base	Conc. (Mol/L)	Stir-ring	Atm	T (°C)	Duration /ageing	Yield [a] (wt%)	Particle Shape TEM	S_{BET} (m^2/g)	L_z/L_{xy} (nm)
SO	CuO-$Cu(NO_3)_2$	No	0.2 0.25	Y	N_2	RT	4 weeks	92	Irregular rod-like. 2µm long-1µm broad	1.4	193/132
$AP_{0,1M\text{-no ageing- RT}}$	$Cu(NO_3)_2$	NaOH	0.1 0.1	Y	N_2	RT	2min	37	Undefined/broken plates. 200nm-1µm	17.5	28/35
$AP_{0,1M\text{-1day- RT}}$	-	-	-	-	-	RT	2min/1day	54	Undefined plates. 1µm	13.3	33/39
$AP_{0,1M\text{-4days- RT}}$	-	-	-	-	-	RT	2min/4days	60	Mixture of small/broken <1µm + large plates 2µm + tiny crystal bits<100nm	10.0	
$AP_{0,1M\text{-4days- 40°C}}$	-	-	-	-	-	40	2min/4days	63	Well dispersed plates, undefined shape. 2µm	10.0	42/44
$AP_{1M\text{-4days- RT}}$	-	-	1 1	-	-	RT	2min/4days	59	Very small platelets <100nm	6.7	
$Urea_{Reflux}$	$Cu(NO_3)_2$	Urea	0.2 0.5	Y	N_2	80	2H	83	Broken pieces of very wide plates. 20µm in-plane/5µm thick	1.8	185/62
$Urea_{HT}$	-	-	-	N	Auto-clave	-	-	27	Radial growth of thick and large plates	1.1	202/52
US_{30min}	$Cu(NO_3)_2$	Urea	0.2 0.5	N	Ar degas. -	RT	30min	7	Well defined rectangu-lar/rhombic plates. 5-10 µm in-plane, <1µm thick	1.5	139/52
US_{150min}	-	-	-	-	-	-	150min	42		1.8	138/79
US_{240min}	-	-	-	-	-	-	240min	54	Large and thick discs. 5-15µm diam., 2 µm thick	<1	178/99
$MWHT_{30\ min\text{-}80°C}$	$Cu(NO_3)_2$	Urea	0.2 0.5	Y	Air	80	30min	5	Mixture of small/broken <5µm + large rectangular plates 10-20µm	2.6	64/51
$MWHT_{\ 60\ min\text{-}80°C}$	-	-	-	-	-	80	60min	2		3.1	75/74
$MWHT_{240\ min\text{-}80°C}$	-	-	-	-	-	80	240min	8	Very well defined rectangu-lar rhombic platelets 10-20µm	<1	157/77
$MWHT_{30\ min\text{-}100°C}$	-	-	-	-	-	100	30min	5	10-30µm	1.3	218/87

[a] Percent yield is the amount of solid obtained with respect to the theoretically expected pure compound amount

EXPERIMENTAL DETAILS

Synthesis. For the synthesis of $Cu_2(OH)_3(NO_3)$ samples, AR grade raw chemicals were used. Copper oxide (CuO, 98%), copper nitrate trihydrate ($Cu(NO_3)_2.3H_2O$, 98%) were purchased from Aldrich, sodium hydroxide (NaOH, 98%) from Acros and urea (CH_4N_2O, 99%) from Prolabo. For synthesis by salt and oxide hydrolysis (SO), 15.9 g of CuO (0.2 mol) were dispersed into 200 mL of a 1.25 Mol/L aqueous copper nitrate solution. The mixture was kept under stirring for 4 weeks under nitrogen atmosphere after which the solid was recovered by centrifugation at 4500 rpm (relative centrifugal force of 3056^xg) washed three times with deionized water and dried at 60°C in oven. For synthesis by alkaline precipitation (AP), 50 mL of a copper nitrate solution (0.1 Mol/L or 1 Mol/L) and 50 mL of NaOH solution (0.1 Mol/L or 1 Mol/L) were added simultaneously in 5 min. into a 1L reactor containing 200 mL of water using peristaltic pumps at a flow rate of 10 $mL.min^{-1}$. The resulting dispersions were kept under stirring and nitrogen atmosphere at room temperature or 40°C for different ageing times (no ageing, 1 day, 4 days) after which the precipitates were recovered by centrifugation (4500 rpm/3056^xg), washed three times with water and dried at 60°C in an oven. For the synthesis by urea hydrolysis, 3g of urea (0.05 mol) were added into 80 mL of a 0.2 Mol/L copper nitrate solution. Then, the mixture was heated at 80°C for 2 hours either by reflux method (Urea reflux) or by hydrothermal treatment (Urea HT) using a teflon coated stainless steel autoclave. In both cases, the precipitates were recovered by centrifugation (4500 rpm/3056^xg), washed three times with water and dried at 60°C in an oven. For microwave hydrothermal treatment (MWHT) synthesis, the same mixture as prepared for urea hydrolysis was poured 80 mL vessels and irradiated with microwaves at a power of 300 W using a Discover® SP-D 80 microwave for different period of times (30 min, 60 min, 240 min) and different temperatures (80°C, 100°C); the pressure reached was around 290 psi. For sonochemical synthesis (US), the same mixture as prepared for urea hydrolysis was also used. After 1 hour stirring at room temperature under nitrogen atmosphere, it was subjected to intense ultrasonic irradiation (20KHz and 21 W/cm^2) during various times (30 min, 150 min, 240 min) using Vibra-Cell™ 75041 equipment. Solids obtained by MWHT and US methods were recovered by centrifugation (4500

rpm/3056xg), washed three times with and dried at 60°C in the oven. The materials were labelled for instance as $AP_{0,1M\text{-}4days\text{-}40°C}$ according to the synthesis method, the concentration of reactants, the reaction or ageing time and the temperature applied.

Materials Characterization. X-ray diffraction (XRD) analysis of the samples were carried out on a Philips X'Pert pro diffractometer equipped with a X'celerator 1D detector (2.122° active length), using CuKα1/ Kα2 source in Bragg Brentano θ-θ geometry from 5 to 90°(2θ) with a scan step of 0.016°. Profile matching and structure refinement were using FullProf suite package.[17] To properly reproduce XRD peak profile and reach good fits, it was necessary to consider microstructural effects in particular anisotropic size effects, related to the platelet morphology of the particles, and these were modelled with linear combinations of spherical harmonics SH as implemented in FullProf. The SH description also allowed the calculation of the volume-averaged apparent size of the coherent domains along each reciprocal lattice vector and to do so, LaB_6 NIST standard was used to correct for instrumental broadening. The plate shape of the crystallites also led us to consider preferred orientation PO effects on the XRD patterns, in the [001] direction as stacking direction of the hydroxide layers. For that, the exponential function as implemented in Fullprof was used and G1/G2 parameters were included after the preliminary refinement with the random orientation of the crystallites had converged. For Rietveld refinements, the atomic positions reported by Effenberger for Rouaite monoclinic polymorph were considered as starting structural model.[18] Only the atomic positions within the hydroxide layer were refined; nitrate anion geometry and N-O bonds were fixed. The atomic PDF were obtained from X-ray total scattering data collected on a PANalytical Empyrean diffractometer equipped with a solid state GaliPIX3D detector, a focusing X-ray multilayer mirror, and an Ag anticathode (Kα1 = 0.5594 Å, Kα2 = 0.5638 Å). The active material powders or electrode paste mixtures recovered after various numbers of charge-discharge cycles were placed in glass capillaries of 0.7 mm diameter. An empty capillary of the same type or only filled with electrode additives were measured in the same way for background subtraction. Data were recorded over the 1-145° 2θ range, which corresponds to an accessible maximum value for the scattering vector Q max of 21.4 $Å^{-1}$. Data merging, background subtraction, and Kα2 stripping were done using HighScore Plus software provided by PANalytical Corporation. It was also used to generate corrected and normalized total scattering structure functions S(Q). Finally, the PDF or G(r) were calculated from the Fourier transforms of S(Q) truncated at 21 $Å^{-1}$. The program PDFgui was used to extract local structural information from the measured PDF.[19] As starting models, we considered the structural data reported by Smura et al.[20] for Cu_2O (COD 1010941), Fortes et al.[21] for Cu (COD 4105040) and Skapski et al.[22] for $Cu(II)_2(O_2CCH_3)4.2H_2O$. Scanning electron microscopy (SEM) images were recorded using a JSM-7500F field-emission scanning electron microscope operating at an acceleration voltage of 3 kV. Samples to be imaged were mounted on conductive carbon adhesive tabs and coated with a gold thin layer. Infrared spectra were recorded in transmission mode using the KBr pellet technique (2 wt. %) with a Nicolet 5700 spectrometer from Thermo Scientific over the wavenumber domain of 400 to 4000 cm^{-1} with a scan number of 128 at a resolution of 4 cm^{-1}. Thermogravimetric analysis (TGA) under air flow in the temperature range of 25–1000 °C with a linear temperature ramp of 5 °C min^{-1}. Surface areas were determined from the BET analysis of nitrogen adsorption isotherms recorded at 77 K using a Micromeritics ASAP 2020.

Electrochemical Measurements. The electrode pastes were prepared mixing LHS/SG/PTFE in a 60/30/10 wt. % ratio. The obtained pastes were dried in the oven at 60°C, then pressed under 5 tons on a steel grid. Cyclic voltammetry (CV) curves were performed using a Biologic VMP3 with a three electrode setup with LSG/SG/PTFE as a working electrode, Ag/AgCl (KCl sat) as a reference and platinum as a counter electrode. The electrolyte was sodium acetate (1 Mol/L) in a [-1.2;1] V potential range.

RESULTS AND DISCUSSION

Synthesis and Morphology Analysis. The characteristics of the samples and the synthesis conditions are summarized in Table 1. It should be noted that US and MWHT methods have been used in very few of the LHS material synthesis reported so far and the results obtained here are therefore highly original. The formation of $Cu_2(OH)_3NO_3$ phases was confirmed in all cases based on XRD analysis, supplemented by TGA and IR analysis given in the Supporting Information (Figure S1 and S2). The crystallization behavior of layered metal hydroxides is usually explained by the classical nucleation and growth model and these materials tend to develop 2D morphologies. Indeed, due to the large difference in the density of atoms between the stacking and lateral directions, the basal crystallographic planes are the dominant exposed facets (Bravais' Law) in layered materials, leading to a growth in the lateral direction to form platelet-like particles.[23] Here, depending on the synthesis method applied, particles with different shapes, sizes, aggregation states and different crystallinity were obtained. SEM images of samples representative of each series are displayed in Figure 1 together with XRD patterns.

As a first method, we applied the hydrolysis of divalent metal salts in the presence of metal oxide (SO method) which has been known for a long time.[24, 25] A weak point for this method is the reaction time that can be very long, thus explaining its underuse. In the present case, the reaction was conducted over four weeks and micro sized particles were obtained with a coarse rod-like shape indicating a directed aggregation of primary platelet crystals in the stacking direction (Figure 1a). Although not discussed in the former studies, such anisotropic crystal growth of layered compounds along the stacking direction is quite unusual and we can attribute it to high supersaturation conditions which are maintained constant over a long period through the controlled release of metal ions from CuO.[26, 27] These conditions also explain the very high product yield achieved by this method, higher than 90 wt.%.

The high purity and crystallinity of the sample enabled a Rietveld refinement of the XRD data (discussed later), and showed a structure similar to the Rouaite mineral.[18] The second method applied was the precipitation (AP) with the simple addition of a hydroxide solution in an acidic aqueous solution containing M^{2+} cations and A^{m-}counter-anions. This is a widely used method for preparing LHS materials with many parameters that can be varied such as the pH, the concentration of the reactants and the addition rate of the solution.**Erreur ! Signet non défini.** In the present case, the quick addition within a few minutes of 0.1M NaOH led to the formation of well dispersed platelets of submicron size with slightly indented contours (Figure 1b). After 96 hours of ageing, the presence of both very small particles and much bigger platelets suggests the occurrence of Ostwald ripening process with the slow disappearance of small platelets in favor of the larger ones.[28] The measured product yields confirm this mechanism with the lowest value obtained for $AP_{0.1M\text{-no ageing-RT}}$ but which increases noticeably upon ageing. An increase in temperature, even as low as 40°C, produced an acceleration of this process, leading to micro-sized homogenous particles with better crystallinity as shown by the comparison of XRD data. On the contrary, the use of 1 Mol/L NaOH led to the formation of many small nuclei due to a rapid rise in pH, but which grew smaller and are much less crystalline, as evidenced by the broad character of XRD peaks. The XRD data also indicate the presence of impurities that do not disappear upon ageing and thermal treatment. In the end, the maximum yield achieved for these two NaOH concentrations is practically the same, in the order of 60 wt%, but with net differences in terms of crystallinity and purity.

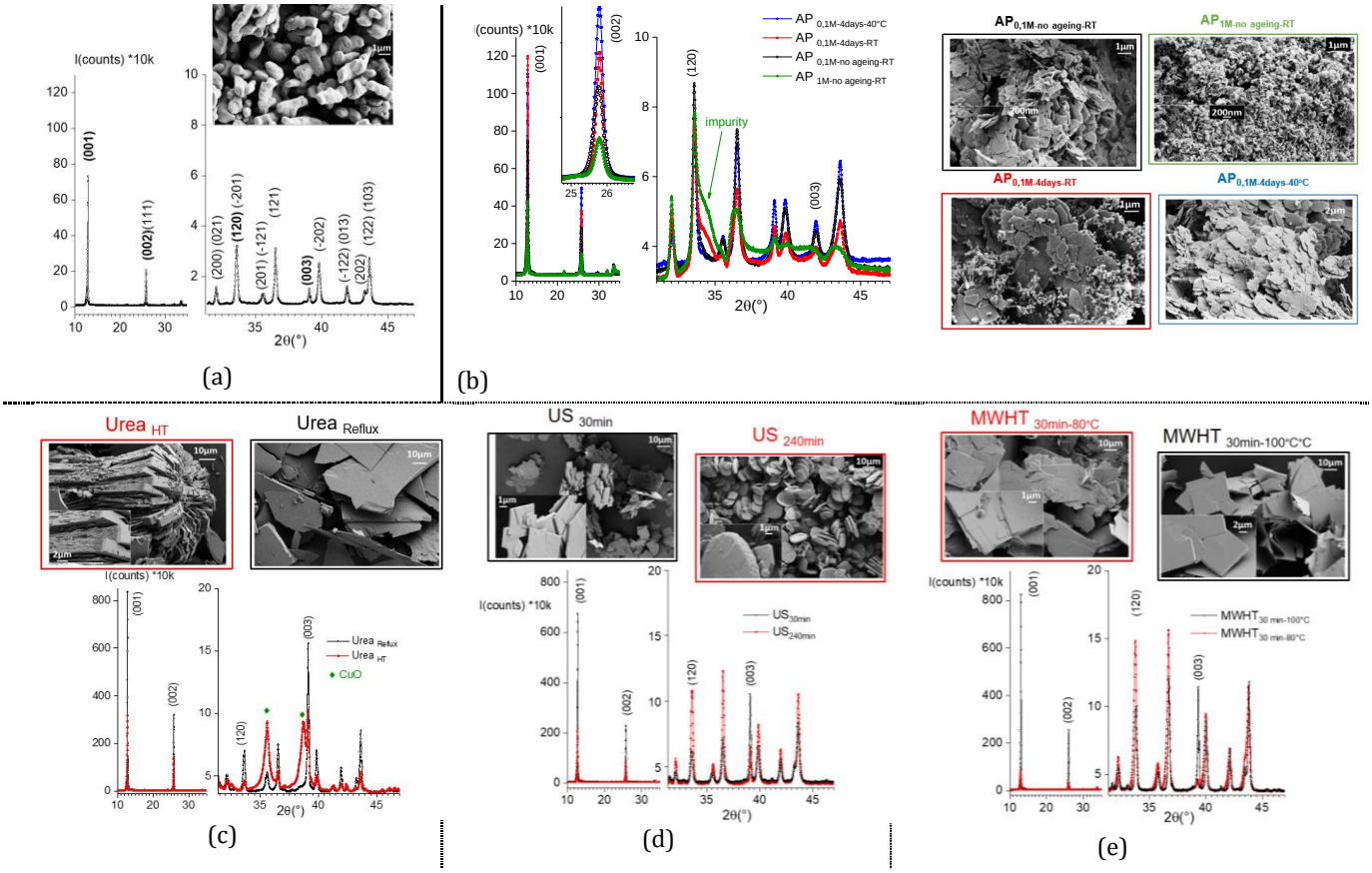

Figure 1. The variation of the morphologies and the XRD patterns of $Cu_2(OH)_3NO_3$ sample series prepared according five different synthesis methods: (a) hydrolysis of salt and oxide (SO), (b) precipitation with alkaline solution (AP), (c) urea hydrolysis (Urea), (d) sonochemistry (US) and (e) microwave hydrothermal treatment (MWHT)

As a third method, urea hydrolysis was used which is less frequent used than the previous two for LHS materials. It is based on the slow hydrolysis of urea providing hydroxide groups for the reaction with the salt solution.[29] CO_2 is also produced which can lead to the formation of carbonate anions and unless it is the desired anions, this can appear as a contamination in the final product. We applied thermal urea hydrolysis at 80°C either under reflux in an oil bath ($Urea_{Reflux}$), or combined with a hydrothermal treatment in a Teflon-lined stainless-steel autoclave ($Urea_{HT}$). As explained in the case of the LDH materials, the progressive hydrolysis of urea upon heating enables nucleation to occur at a slow rate (low supersaturation conditions) which is favorable to the growth of very large platelets.[29] In the present case, platelets of several dozen of microns size with a sharp contour, were easily attained under reflux at 80°C within just 2 hours (Figure 1c). Interestingly, assemblies of platelets, arranged in an apparently cylindrical manner (radial morphology) with *ca* 15–20 microns in diameter were obtained under hydrothermal treatment,

that are likely to emanate from a common nucleus. The highly anisotropic character of the particles is visible on the XRD patterns with very intense 00*l* basal reflections relative to non-basal *hk* reflections, for instance 120. This preferential orientation is prominent for the sample obtained by reflux heating that also shows better crystallinity with very narrow XRD peaks and a good product yield, higher than 80 wt%. The yield is considerably decreased upon hydrothermal heating, lower than 30 wt% and XRD analysis indicates the presence of CuO. The absence of stirring in the autoclave vessel used and a too short heating time are likely explanatory factors.

For the last two methods applied, urea hydrolysis was coupled with an ultrasonic treatment (US method), and a microwave-hydrothermal treatment (MWHT). Since the reactants and the concentrations were the same in both synthesis, a direct comparison can be done between these the two methods and urea hydrolysis described above. Sonochemistry has been applied very little for the synthesis of LHS so far. Using a high-intensity ultrasonic horn (20 kHz, 100/50 $W.cm^{-2}$), the generation of OH° radicals by the sonolysis of water was reported to lead first to the formation of Cu(0)/ Cu_2O particles which then react with NO_3^- to form LHS copper hydroxide nitrate.[30, 31] In the present case, a lower power intensity was applied (20 kHz, 21 W. cm^{-2}) and we did not observe the formation of any reduced Cu species but it clearly accelerated the formation of $Cu_2(OH)_3NO_3$ in only 3 min. Hot spots generated by acoustic cavitation induced homogeneous nucleation and crystallization of very well-defined rectangular platelets of a few microns as can be seen in Figure 1d with some intergrowth sites visible. Interestingly, by increasing the sonication time, the rectangular platelets stack and align side by side, then fused together, as in a sintering process, leading to very large disc-shaped particles with a diameter of about ten microns and a thickness a few microns (US_{240min}), never reported so far. One can attribute this disc shape outline to high velocity impacts between particles driven by ultrasounds.[32] The synthesis yield also increases significantly with the sonication time, reaching values comparable to the AP method after a sonication time of 150 min but with a much higher crystallinity. The last method applied was microwave hydrothermal treatment (MWHT). As already reported in the literature, both nucleation and crystal growth can be considerably accelerated by combining microwave dielectric heating and hydrothermal conditions due to uniform bulk heating and an increased solubility and reactivity of reactants.[33] This method has never been applied as such to LHS synthesis so far; the only studies available concern microwave-assisted post-synthesis modifications of LHS.[34] The reasons are probably some drawbacks similar to those reported by using MW for LDH materials ie ZnO phase formation/segregation when Zn^{2+} cations are involved, an accelerated oxidation process of Co^{2+} or Mn^{2+} cations…[35] In the present case, we did not observe any contamination in the final product, even for long microwave irradiation times up to 240 min. While at 60°C no product was formed, very large platelets of submicron-thick and in-plane dimensions of several microns were obtained at 80°C for an irradiation time of only 30 min (Figure 1e). The intergrowth of more uniform rectangular platelets of tens micron wide was observed at 100°C after an irradiation time of 30 min, also displaying a better crystallinity. However, the significant reduction in synthesis time is counterbalanced by very low product yields, lower than 10 wt%. Such a low synthesis yield is of course an important issue to address, by optimizing the MW field homogeneity, MW power, volume/stirring of reaction system, heating rate/ temperature/ time etc. but this was beyond the scope of this study.

In addition to SEM images, BET analysis (Figure S3) was used to further characterize the textural properties of LHS materials. Nitrogen adsorption/desorption isotherms indicate the formation of non-porous materials with a very small surface area (Table 1); no hysteresis loops attributable to mesoporous interparticle pores were detected either. The slight differences observed here only arise from differences in particle size and dispersion/aggregation state. Hence, the surface area of AP samples, composed of small and well dispersed particles, is larger (~10-20 m^2/g) than that measured for the other sample series displaying much bigger particles (< 3 m^2/g). Highly crystalline samples such as US_{240min}, $MWHT_{240min\text{-}80°C}$ even have no measurable specific surface area.

Structural and Microstructural Analysis. Copper hydroxide nitrate in its anhydrous form is known to occur in two polymorphic forms, orthorhombic ($P2_12_12_1$) and monoclinic ($P2_1/m$) forms that refer to Gerhardtite and Rouaite crystal minerals, respectively.[18, 36] Both structures are derived from $Cu(OH)_2$ with strongly edge bonded Jahn-Teller distorted Cu^{2+} octahedra coordinated to six hydroxide anions; one-quarter of the hydroxides are replaced by nitrate anions, which point alternately outside the layers, connected through N–O bonds (Figure 2). The only difference between the two structures is in the orientation of the NO_3 with a constrained orientation for the monoclinic polymorph and a free orientation in the case of orthorhombic polymorph. The monoclinic polymorph is considered as a metastable phase who's synthesis is kinetically favoured.[31] These two polymorphs are rather difficult to distinguish based on XRD patterns, but one noticeable difference however concerns the second most intense peak at ca 25.77° (2θ) which in the case of the monoclinic polymorph is the contribution of two *hkl* reflections, *i.e.* 002 and 111, leading to an XRD peak with a right shoulder, while in the case of the orthorhombic polymorph, a single peak is expected attributed to 040 (Figure 3). In the present case, the formation of the monoclinic polymorph was confirmed by XRD data for all the methods of synthesis applied.

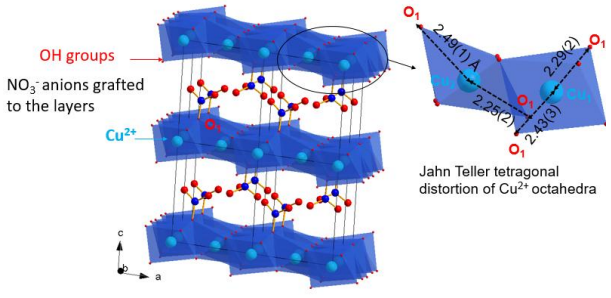

Figure 2. Polyhedral representation of the copper hydroxide nitrate monoclinic structure obtained from Rietveld refinement parameters for US_{150min} sample

Most of the samples appear to consist of pure LHS single phases and it was possible to perform Rietveld refinements of the powder XRD data for many of them. Details are given in Supporting Information with refinement results in Table S1 and Figures S4, refined atomic parameters in Table S2 and main distances within the hydroxide layers and in the interlayer space in Table S3. As an example, the graphical output of the Rietveld refinement for US_{150} sample is displayed in Figure 3. A few remarks can be made for some samples, first for AP_{1M} samples for which no refinement could be conducted, nor even a profile refinement, due to important peak profile anisotropy and the presence of an amorphous component that could not be identified but assumed to be a copper oxy-hydroxide. On the other hand, for Urea samples, CO_2 produced by urea hydrolysis led to the formation of Malachit $Cu_2(OH)_2CO_3$ in small amounts < 2 wt% and the application of the hydrothermal treatment resulted in the formation of CuO up to 6 wt%.

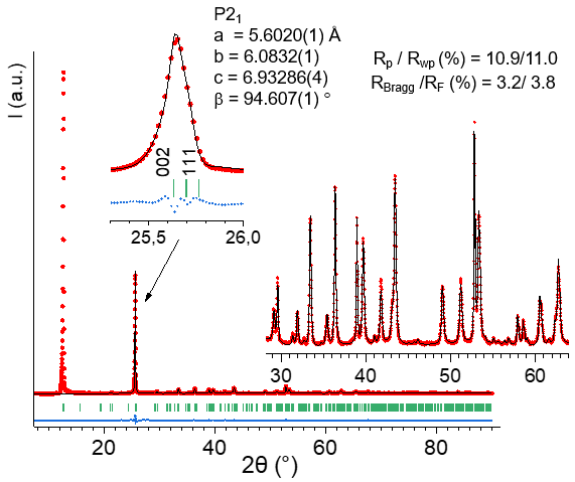

Figure 3. Graphical results of the Rietveld refinement for US_{150min} sample. Experimental X-ray diffraction pattern (red cross), calculated pattern (solid black line), Bragg reflections (green ticks), and difference profile (solid blue line). The quality of the fit is more visible in the insets. The fitting of the peak at 25.77 °(2θ) with the contributions of both 002 and 111 reflections is consistent with the monoclinic polymorph. Low Bragg angle range (20 < 10°) was excluded from the refinement because it contains the strongest peak which is most affected by experimental errors and may strongly influence the refinement.

The differences observed between samples in terms of crystallinity can be further characterized by X-ray diffraction line profile analysis which enables the size of individual perfect crystalline domains within particles to be determined. Using the anisotropic spherical harmonic size approach, the coherence lengths along all crystallographic directions can be calculated. In the present case, we were particularly interested in the [00l] and [120] directions, reflecting the extent of the structural coherence length along the stacking direction (L_z) and in the plane of the hydroxide layers (L_{xy}), respectively. The values are reported in Table 1 and indicate the initial formation of nanosized primary particles ranging from c.a. 25 to 200 nm. Therefore, the (sub)micro-sized particles observed by SEM must be considered as polycrystalline secondary particles resulting from the growth by orientated aggregation of the above primary nanoparticles. It can also be noted that the large particles seen by SEM are made up of large crystalline domains.

Interesting differences are observed concerning the shape anisotropy of the crystalline domains measured through the crystal aspect ratio L_z/L_{xy} of thickness to lateral size. At first sight, it might be expected that particle morphologies would originate from crystalline domains of similar shape ie L_z/L_{xy} <1 for platelets and L_z/L_{xy} >1 for rod-like particles. For SO and AP particles, it appears that growth follows the shape of the primary crystallites with a L_z/L_{xy} value of 1.6 for SO rod-shaped particles and 0.8 to 1.0 for AP platelets. On the other hand, for the other sample series displaying L_z/L_{xy} values from 1.6 to 3.5, the aggregative growth occurs in the opposite direction (lateral direction) than expected from crystalline domains (stacking direction). It is thus inferred that the dominant exposed facets must remain basal crystallographic planes (ab-planes) and crystal growth occurs in the lateral direction to form plate-like particles.

Electrochemical behavior. The electrochemical behavior of all samples was investigated using a three-electrode setup through cyclic voltammetry CV in 1M $NaCH_3COOH$ aqueous solution as an electrolyte and a wide potential window from -1.2V to 1V vs Ag/AgCl in order to follow all the transformations undergone by the material. This wide potential range induces a water electrolysis reaction. One hundred CVs were recorded for each sample with significant peak shifts and differences in the peak area indicating important changes upon cycling. Even if we note some differences depending on the synthesis method, CV plots are rather similar among all samples (Figures 4 and S5). Copper redox peaks are clearly observed in the first scan attributed Cu(II)/Cu(I) and Cu(I)/Cu(0) couples. As shown in the case of LDH and also applies to the case of other layered materials, the reversible oxidation/reduction of the cations within the hydroxide layers induces changes in the interlayer space with a release of the interlayer anions and the intercalation of the anions electrolyte.[37] A delamination of the layers may also occur.

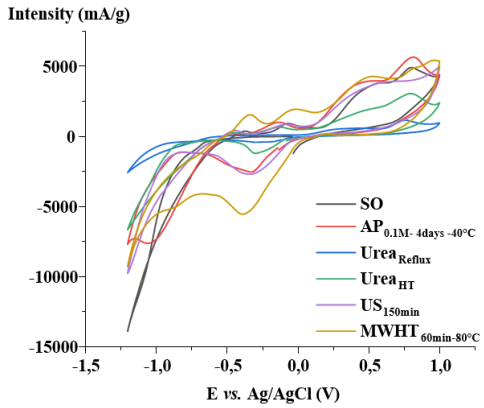

Figure 4. First cyclic voltammetry for $Cu_2(OH)_3(NO_3)$ sample series, measured in 1 Mol/L sodium acetate at 10mV/s

The discussion first focus on the CV curves of the first cycle since it refers to the starting composition *ie* $Cu_2(OH)_3(NO_3)$. The CV curves (first cycle) at a scan rate of 10 mV/s for representative samples of each synthesis method are displayed in Figure 4. Direct capacities were determined from these CV curves and are given in Figure S6. These experimental values can be compared to the theoretical capacity of $Cu_2(OH)_3(NO_3)$ calculated according to this equation: $Q\left[\frac{mAh}{g}\right] = \frac{\Delta x\ F}{M*3.6}$ where, Δx is the number of electrons exchanged, F Faraday constant in As/mol, and M the molar mass of the compound in g/mol. Thus, assuming a two electrons transfer, owing to the ability of copper (II) to be reduce to Cu metal, a theoretical capacity of 223 mAh/g should be obtained. The best capacity at the 1st cycle is observed for AP samples with a value of 197 mAh/g for $AP_{0.1M\text{-}4days\text{-}40°C}$ which corresponds to 88% of the maximum capacity expected for $Cu_2(OH)_3(NO_3)$ if we assume that there is no contribution from water electrolysis. Such a high capacity close to the theoretical one supports the presence of bulk redox reactions not only limited to the surface of the material at the beginning of the cycling. Thus, the percentage of copper atoms affected by the electrochemical process ranges from 88% for $AP_{0.1M\text{-}4days\text{-}40°C}$ to 25% for SO. Interestingly, the capacities measured on the first cycle can be related to the size of the crystalline domains determined above as shown in Figure 5 and Figure S7. Based on the L_z/L_{xy} ratio, the materials can be divided into three groups: those very well crystallized both in the in-plane and stacking directions leading to a L_z/L_{xy} ratio between 1 and 2 (Group 1); those also well crystallized but more in the stacking direction leading to a ratio of $L_z/L_{xy}>2$ (Group 2), and finally those much less crystallized with small coherent domains in particular in the stacking direction leading to a ratio of $L_z/L_{xy}<1$ (Group 3).

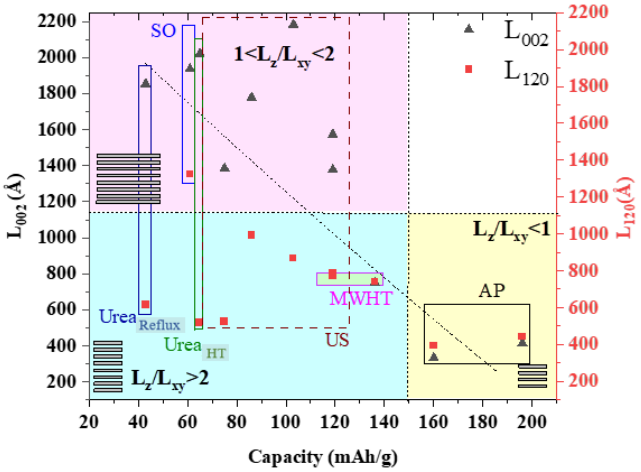

Figure 5. Correlation between the capacities obtained from CV of first cycle and structural coherence lengths L_z and L_{xy} obtained from XRD analysis for $Cu_2(OH)_3(NO_3)$ sample series.

Clearly the capacities are much higher for this latter group indicating an influence of nanostructure size and morphology on LHS electrochemical properties. The beneficial effect of nanostructuration on active surface sites giving rise to superior electrochemical performances has been documented in many studies.[38] Additionally, the 2D nanostructure morphology of AP particles is expected to have the highest surface to volume ratio providing even more active surface sites. This study of L_z/L_{xy} ratio also suggests that stacking order could have an unfavorable effect on the electrochemical properties. Indeed, long stacking coherence lengths are synonymous of stacking stability and we believe this results in poor diffusion properties in the interlayer space, thus preventing the anion electrolyte intercalation and deintercalation reactions during the electrochemical process.[39]

Cycling stability measurements for up to 100 cycles show the influence of the average apparent size of the crystalline domains on the capacity stability and the occurrence of phase transformation (Figure S8). Thus, small particles such as AP particles show a rapid loss of capacity in the initial cycles (80 % capacity loss after 100 cycles for AP) while larger particles show a more gradual capacity decrease. Yet, after 100 cycles, all the samples tend to the same capacity of *ca* 40 mAh/g. It is believed that the small particles with a large interfacial area provide more active sites which in return accelerate phase transformation. Additionally, an electrochemical grinding from the edges of the particles to the core. The same phase transformation occurs in all samples during electrochemical cycling but is delayed depending on the particle size. US and MWHT samples belonging to the Group 1 L_z/L_{xy} ratio between 1 and 2 and displaying large particle sizes can represent a good compromise between capacity and cycling stability retaining up to 30% and 40 % respectively of their original capacity at 100 cycles.

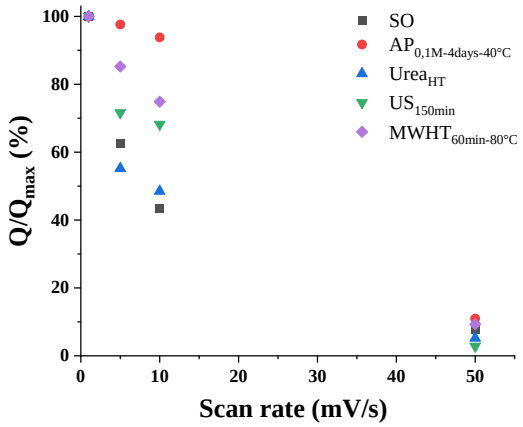

Figure 6. Evolution of Q/Q_{max} depending on scan rate for $Cu_2(OH)_3(NO_3)$ sample series, measured in 1 Mol/L sodium acetate at 1st cycle.

By varying scan rate in cyclic voltammetry and by plotting the evolution of the Q/Q_{max} ratio with Q_{max} the capacity obtained at 1mV/s (Figures 6 and S9), it is possible to distinguish the impact of morphology on capacity. These data clearly indicate that the electrochemical process is not purely controlled by the surface and that the electrochemical reaction is diffusion limited, because at high scan rates (50 mV/s), less than 10% of Q_{max} was reached for all synthesis. But AP sample provides 93% of Q_{max} at 10mV/s in comparison with SO sample which give 62%. That is a direct consequence of morphology and nanostructuration.

Phase transformations during cycling. Structural changes that occur during cycling were investigated through X-ray pair distribution function analysis carried out on SO sample recovered after 1, 10, 100 and 500 complete cycles and at 0V vs Ag/AgCl (Figure 7). PDF, as a total scattering technique, probes both the crystalline and amorphous phases and is an interesting tool in structural evolution study of electrode materials.[40] Using PDFgui software we were able to extract quantitative structural information. It was thus shown that $Cu_2(OH)_3(NO_3)$ rapidly undergoes transformation into cuprous oxide Cu_2O (cycle 10). Then, the disproportionation reaction of $Cu(I)_2O$ in acetate electrolyte can easily explain the formation of the dimeric copper(II) acetate monohydrate $Cu(II)_2(O_2CCH_3)_4.2H_2O$ as observed at cycle 100 and also the formation of Cu(0) clearly visible at cycle 500. The compositions of the electrode materials in weight % deduced from PDF modelling are the following: 100% Cu_2O (cycle 10), 36% Cu_2O – 64% Cu acetate (Cycle 100) and 51% Cu_2O – 15 % Cu- 34% Cu acetate (Cycle 500).

The changes in pH were measured during cycling (Figure S10) and it is quite interesting to note that the pH values measured at potential values -1.2, 0 and 1V vs Ag/AgCl on successive CV cycles for SO sample and placed on the Pourbaix diagram of Cu-H_2O-acetate (Figure S11) allow a better understanding of material transformations and PDF results. This allows us to propose the following sequence of reactions (equations 1–4). The present system is, however, a very heterogeneous solid system, composed of domains more or less exposed to the electrochemical process which departs from the ideality of Pourbaix's diagram. First, it is worth noting that the stability of $Cu_2(OH)_3(NO_3)$ in 1M sodium acetate at pH 8.2 was checked over a period of 24 h (Figure S12). After 10 cycles, all the LHS is reduced according to Equation1. This first hypothesis is supported by the increase of pH following to the release of hydroxyl group in the solution. Then, the Cu_2O is reduced to Cu metal at negative potentials based on Equation 2. At around -0.8V vs Ag/AgCl water reduction occurs following Equation 3, also accompanied by a release of OH- species. In addition, Figure 8 clearly shows hydrogen evolution from 0.8V vs Ag/AgCl after 10 cycles. This hydrogen evolution decreases with more cycles, probably due to passivation of the copper, or there is no more copper formation.

$$Cu_2(OH)_3(NO_3) + 2e^- \rightarrow Cu_2O + OH^- + NO_3^- + H_2O \quad (1)$$

$$Cu_2O + H_2O + 2e^- \rightarrow 2Cu + 2OH^- \quad (2)$$

$$2H_2O + 2e^- \rightarrow H_2 + 2OH^- \quad (3)$$

On the return scan, as the applied potential becomes positive, the transformation of copper metal to cuprous oxide is observed first at -0.2V *vs.* Ag/AgCl). We did not observe the transformation of cuprous oxide to cupric (expected according Pourbaix's diagram) in the potential range between 0.15 to 1 *V* oxide takes place. After a few dozen cycles, in particular at 50th cycle, a new phase appears which is Cu(II) acetate $Cu(II)_2(O_2CCH_3)_4.2H_2O$. We can draw a parallel between our results and the study reported by Karantonis and al.[41] on the anodic oxidation of copper. The formation of cuprous oxide on the electrode surface was followed by extensive dissolution mainly in the potential region where Cu(II) monoxide layers is likely to be formed. It was also established that the role of acetate ions is not limited to the adjustment of the pH but are also involved in the formation of basic copper acetate $Cu(II)_2(O_2CCH_3)_4.2H_2O$.

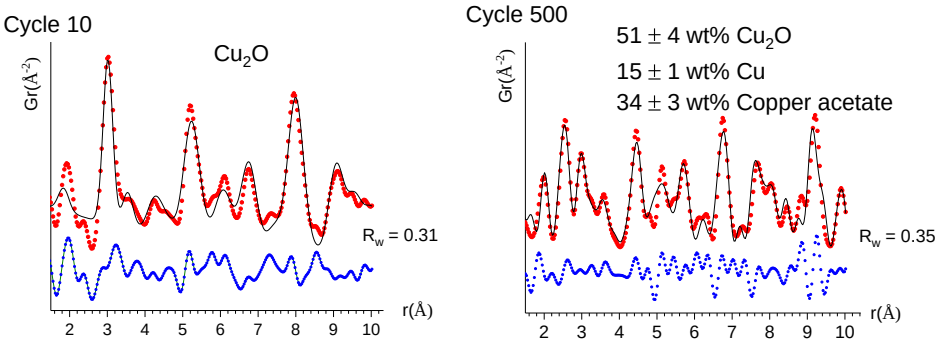

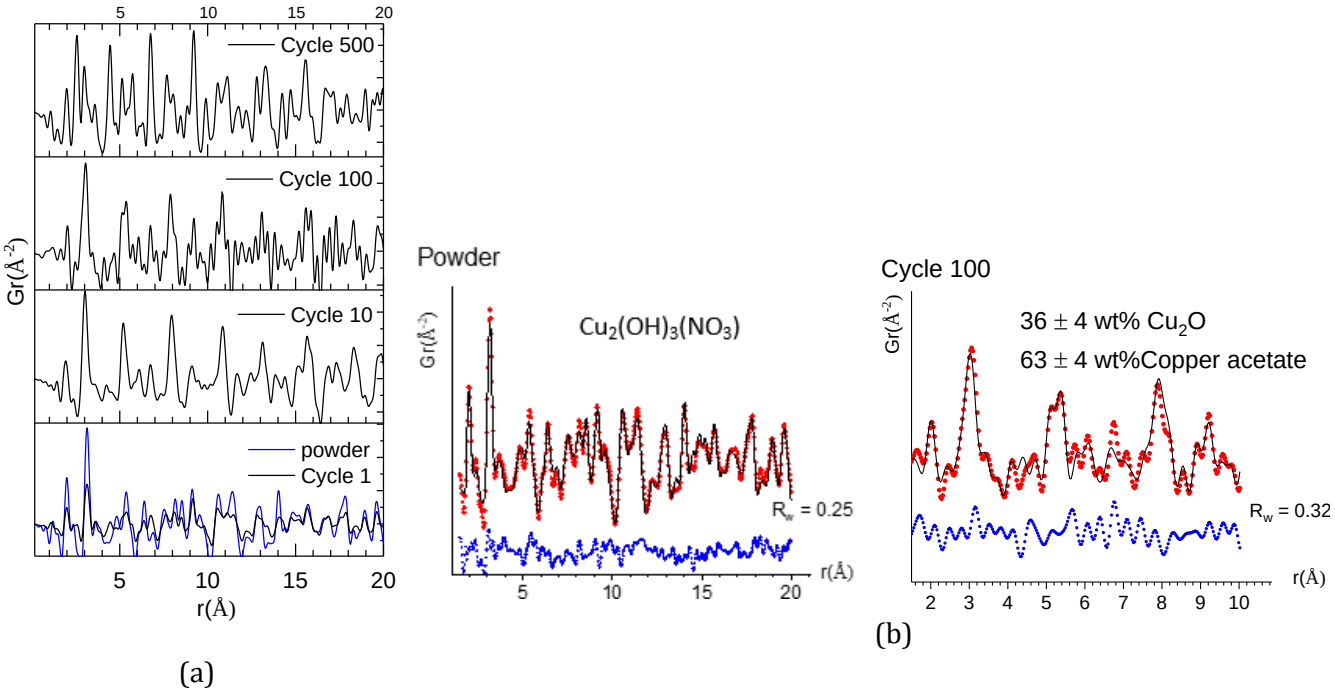

Figure 7. (a) PDF data electrode materials for SO sample after 1, 10, 100 and 500 complete CV cycles. (b) Fitting of the very local structure 1.5 <r<10 Å: experimental data are red stars, fits are black curves and the difference is below in blue.

If we return to the CV curves (Figure 8), at the 100th cycle, three reductions peaks (-0,25V; 0,5V and -0.88V) and two oxidation peaks (-0,62V and -0.44V) are observed that can be attributed to Cu(0)/Cu(I) and Cu(I)/(Cu(II) transitions. At the 250th cycle, we observe a net increase in the cathodic peak current densities and two anodic at -0,23Vand -0.55V indicating a change in the proportion of the phases. At 500th a single reversible redox peak is measured at -0.25V and -0.52V attributed Cu(II)/Cu(I) transition. The capacity loss is important during the first 50 cycles and then stabilizes around 40 mAh/g (Figure S6). This decrease of capacity is direct consequence of phase transformation together with electrochemical grinding. We also assume that part of the material transformed into Cu metal is no longer subject to reversible redox processes. Finally, regardless of the method of synthesis of $Cu_2(OH)_3(NO_3)$, the similar capacity values observed at the 100th cycle all around 40 mAh/g strongly suggest a similar phase mixture *i.e* $[(Cu_2(OAc)_4.2H_2O)_{1-x-y}(Cu)_x(Cu_2O)_y]$. After a high number of cycles, the electrochemical grinding is likely to annihilate the initial microstructural and morphological differences.

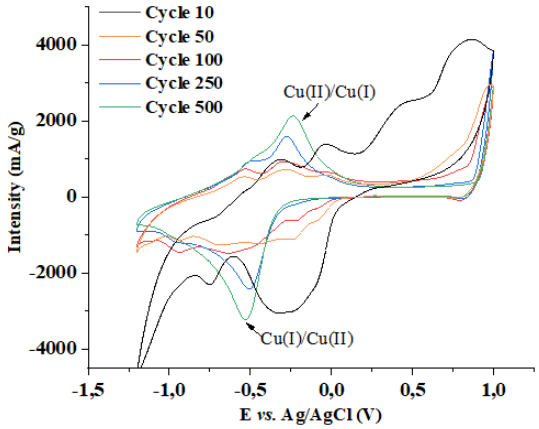

Figure 8. cyclic voltammetry of 10, 50, 100, 250 and 500th cycles of $Cu_2(OH)_3(NO_3)$ SO sample at 10 mV/s in 1 Mol/L sodium acetate.

CONCLUSION

In this study, we first explored different methods of synthesis for the preparation of $Cu_2(OH)_3(NO_3)$ LHS, of which two methods, the sonication and microwave methods, are original. Significant effects were observed on the nanostructure size and particle morphology and comprehensively investigated including the determination of the structural coherence lengths along the stacking direction (L_z) and in the plane of the hydroxide layers (L_{xy}). The electrochemical activity of $Cu_2(OH)_3(NO_3)$ was examined by cyclic voltammetry and clearly shows a beneficial effect of nanostructuration on the capacities measured on the first cycles. Those recorded for nanostructured submicron

AP particles displayed the smallest crystalline domains and reached nearly 90% of the theoretical capacity for a two-electron redox process with a capacity of 197 mAh/g (assuming there is no water electrolysis). Unfortunately, the electrochemical stability of this compounds is poor and the capacity rapidly drops, which makes it unsuitable for any storage application at this stage.

It was also shown that stacking order would have an adverse effect on the electrochemical properties, by limiting the access of the electrolyte to the interlayer space. On the other hand, cycling stability is more dependent on particle size and for this reason, US and MWHT samples formed of nanosized crystalline domains, but agglomerated in micron-sized particles, may represent a good compromise between capacity and cyclability. The loss of capacity is mainly attributed to successive phase transformations into Cu_2O, Cu metal and copper(II) acetate as evidenced by PDF analysis performed on electrode materials after repeated cycling. This probably contributes to an electrochemical grinding which is why all the samples tend to the same capacity of ca 40 mAh/g after the 100^{th} cycle.

SUPPORTING INFORMATION

FTIR spectra, TGA curves, BET analysis, Rietveld refinements results of PXRD data, cyclic voltammetry curves, capacity evolution curves, measurement of pH changes and Cu-H_2O-acetate Pourbaix diagram are available in supporting information files.

AUTHOR INFORMATION

Corresponding Author

***Christine Taviot-Guého.** orcid.org/0000-0002-9468-2684. Email: christine.taviot-gueho@uca.fr

Present Addresses

Camille Douard - Nantes Université, CNRS, Institut des Matériaux de Nantes Jean Rouxel, IMN, 2 rue de la Houssinière BP32229, 44322 Nantes cedex 3, France. Réseau sur le Stockage Electrochimique de l'Energie (RS2E), CNRS FR 3459, 33 rue Saint Leu, 80039 Amiens Cedex, France.

Insaf Gaalich - Nantes Université, CNRS, Institut des Matériaux de Nantes Jean Rouxel, IMN, 2 rue de la Houssinière BP32229, 44322 Nantes cedex 3, France. Réseau sur le Stockage Electrochimique de l'Energie (RS2E), CNRS FR 3459, 33 rue Saint Leu, 80039 Amiens Cedex, France.

Thierry Brousse - Nantes Université, CNRS, Institut des Matériaux de Nantes Jean Rouxel, IMN, 2 rue de la Houssinière BP32229, 44322 Nantes cedex 3, France. Réseau sur le Stockage Electrochimique de l'Energie (RS2E), CNRS FR 3459, 33 rue Saint Leu, 80039 Amiens Cedex, France.

Gwenaëlle Toussaint - EDF R&D, Department LME, Avenue des Renardières, 77818 Morêt-sur-Loing Cedex, France. Réseau sur le Stockage Electrochimique de l'Energie (RS2E), CNRS FR 3459, 33 rue Saint Leu, 80039 Amiens Cedex, France.

Philippe Stevens - EDF R&D, Department LME, Avenue des Renardières, 77818 Morêt-sur-Loing Cedex, France. Réseau sur le Stockage Electrochimique de l'Energie (RS2E), CNRS FR 3459, 33 rue Saint Leu, 80039 Amiens Cedex, France.

ACKNOWLEDGMENT

Authors would like to thanks the French National Research Agency (ANR-20-CE05-0024, LaDHy project) and Labex STORE-EX (ANR-10-LABX-76-01) for financial support.

REFERENCES

(1) Nakagaki. S ; Machado, G. S.; Stival, J. F.; dos Santos, E. H.; Silva, G. M.; Wypych, F. Natural and synthetic layered hydroxide salts (LHS): Recent advances and application perspectives emphasizing catalysis. *Prog. Solid State Chem.* **2021**, 64, 100335-100366

(2) Wang, G; Zhang, L; Zhang, J. A review of electrode materials for electrochemical supercapacitors. *Chem. Soc. Rev*. **2012**, 41, 797–828

(3) Deng, W; Ji, X; Chen, Q; Banks, C. E. Electrochemical capacitors utilising transition metal oxides: an update of recent developments. *RSC Adv.* 2011, 1, 1171–1178.

(4) Rogez, G; Massobrio, C.; Rabu, P.; Drillon, M. Layered hydroxide hybrid nanostructures: a route to multifunctionality. *Chem. Soc. Rev*. **2011**, 40, 1031–1058.

(5) Demel, J.; Lang, K. Layered Hydroxide–Porphyrin Hybrid Materials: Synthesis, Structure, and Properties. *Eur. J. Inorg. Chem.* **2012**, 5154–5164.

(6) Schmid, H; Eisenreich, N. Investigation of a Two-Stage Airbag Module with Azide-Free Gas Generators. *Propellants Explos. Pyrotech*. **2000**, 25, 230-235

(7) Wang, Z; Su, F.; Madhavi, S.; Lou, X. W. CuO nanostructures supported on Cu substrate as integrated electrodes for highly reversible lithium storage. *Nanoscale* **2011**, 3, 1618–1623.

(8) Switzer, J. A.; Kothari, H. M.; Poizot, P.; Nakanishi, S.; Bohannan, E. W. Enantiospecific electrodeposition of a chiral catalyst. *Nature* **2003**, 425, 490–493.

(9) Kim, H; Jin, C.; Park, S.; Kim, S.; Lee, C. H2S gas sensing properties of bare and Pd functionalized CuO nanorods. *Sens. Actuators* **2012**, B 161, 594–599.

(10) Kim, Y. S.; Hwang, I. S.; Kim, S. J.; Lee, C. Y.; Lee, J. H. CuO nanowire gas sensors for air quality control in automotive cabin. *Sens. Actuators* **2008**, B 135, 298– 303.

(11) Sahay, R.; Suresh Kumar, P; Aravindan, V.; Sundaramurthy, J.; Chui Ling, W.; Mhaisalkar, S. G.; Ramakrishna, S.; Madhavi, S. High aspect ratio electrospun CuO nanofibers as anode material for lithium-ion batteries with superior cycleability. *J. Phys. Chem*. C **2012**, 116, 18087–18092.

(12) Zhang, Z.; Chen, H.; She, X.; Sun, J.; Teo, J.; Su, F. Synthesis of mesoporous copper oxide microspheres with different surface areas and their lithium storageproperties. *J. Power Sources* **2012**, 217, 336–344.

(13) Dubal, D.P.; Dhawale, D. S.; Salunkhe, R. R.; Jamdade, V. S.; Lokhande, C. D. Fabrication of copper oxide multilayer nanosheets for supercapacitor application. *J. Alloys Compd*. **2010**, 492, 26–30.

(14) Patake, V. D.; Joshi, S. S.; Lokhande, C. D.; Joo, O. S. Electrodeposited porous and amorphous copper oxide film for application in supercapacitor. *Mater. Chem. Phys*. **2009**, 114, 6–9.

(15) Pendashteh, A.; Mousavi, M. F.; Rahmanifar, M. S. Fabrication of anchored copper oxide nanoparticles on graphene oxide nanosheets via an electrostatic coprecipitation and its application as supercapacitor. *Electrochim. Acta* **2013**, 88, 347–357.

(16) Eyele-Mezui, S.;´ Vialat, P.; Higy, C.; Bourzami, R.; Leuvrey,´C.; Parizel, N.; Turek,P.; Rabu, P.; Rogez, G.; Mousty, C. Electrocatalytic Properties of Metal Phthalocyanine Tetrasulfonate Intercalated in Metal Layered Simple Hydroxides (Metal: Co, Cu, and Zn). *J. Phys. Chem. C* **2015**, 119, 23, 13335–13342.

(17) Rodriguez-Carvajal,J. Recent developments of the program FULLPROF, commission on powder diffraction. *IUCr Newsl.*, **2001**, 26, 12-19.

(18) Effenberger, H. Verfeinerung der Kristallstruktur des monoklinen Dikupfer(II)-trihydroxi-nitrates $Cu_2(NO_3)(OH)_3$. *Z Kristallogr*. **1983**, 165, 127-135.
(19) Farrow, C. L., Juhás, P., Liu, J. W., Bryndin, D., Božin, E. S., Bloch, J., Proffen, T.H. and Billinge, S. J. L. PDFfit2 and PDFgui: computer programs for studying nanostructure in crystals. *J. Phys : Condens. Matter*. **2007**, 19, 335219.
(20) Smura, C.F.; Parker, D.R.; Zbiri, M.; Johnson, M.R.; Gál, Z.A.; Clarke, S.J. High-Spin Cobalt(II) Ions in Square Planar Coordination: Structures and Magnetism of the Oxysulfides $Sr_2CoO_2Cu_2S_2$ and $Ba_2CoO_2Cu_2S_2$ and Their Solid Solution. *J. Am. Chem. Soc.* **2011**, 133, 8, 2691–2705.
(21) Fortes, A. D.; Suard E.;, Lemée-Cailleau, M.H.; Pickard, C.J.; Needs, R.J. Crystal Structure of Ammonia Monohydrate Phase II. *J. Am. Chem. Soc.* **2009**, 131, 37, 13508–13515.
(22) Karantonis, A.; Gerostathi, I.M.; Bourbos, E.; Kouloumbi, N. Corrosion and passivity of copper in basic solutions of acetate ions. *Chem. Eng. Trans*. **2014**, 41, 295-300.
(23) Donnay, J. D. H.; Harker, D. A new law of crystal morphology extending the Law of Bravais. *Am. Mineral.* **1937**, 22, 446–467.
(24) Meyn, M.; Beneke, K.; Lagaly, G. Anion-Exchange Reactions of Hydroxy Double Salts. *Inorg. Chem*. **1993**, 32, 1209-1215.
(25) Rouba, S; Rabu, P.; Drillon,M. Synthesis and Characterization of New Quasi-One-Dimensional Mn(II) Hydroxynitrates $(Mn_xZn_{1-x})(OH)(NO_3)H_2O$ (x = 0.53, 1.00). *J. Solid State Chem*. **1995**, 118, 28-32
(26) Muramatsu, K.; Jimba, M.; Yamada, Y.; Wada, H.; Shimojima, A.; Kuroda, K. Anisotropic Crystal Growth of Layered Nickel Hydroxide along the Stacking Direction Using Amine Ligands. *Inorg. Chem*. **2022**, 61, 8490–8497.
(27) Henrist, C.; Traina, K.; Hubert, C.; Toussaint, G.; Rulmont, A.; Cloots, R. Study of the morphology of copper hydroxynitrate nanoplatelets obtained by controlled double jet precipitation and urea hydrolysis. *J. Cryst. Growth* **2003**, 254, 176–187.
(28) Wagner, C. Theorie der alterung von niederschlägen durch umlösen (Ostwald-reifung). *Z. Elektrochem*. **1961**, 65, 581–591
(29) Hibino, T.; Ohya, H. Synthesis of crystalline layered double hydroxides: Precipitation by using urea hydrolysis and subsequent hydrothermal reactions in aqueous solutions. *App. Clay Sci*. **2009**, 45, 123–132
(30) Anandan, S.; Wu, J. J.; Ashokkumar, M. Sonochemical Synthesis of Layered Copper Hydroxy Nitrate Nanosheets. *Chem. Phys. Chem*. **2015**, 16, 3389 – 3391
(31) Wang, S.; Zhang, X.; Pan, L. Zhao, F. M.; Zou, J. J.; Zhang, T. Controllable sonochemical synthesis of $Cu_2O/Cu_2(OH)_3NO_3$ composites toward synergy of adsorption and photocatalysis. Wang, L. *Appl. Catal. B: Env*. **2015**, 164, 234–240.
(32) Prozorov, T.; Prozorov, R.; Suslick, K.S. High Velocity Interparticle Collisions Driven by Ultrasound. *J. Am. Chem. Soc.* **2004**, 126, 13890-13891.
(33) Zhu, Y. J.; Chen, F. Microwave-Assisted Preparation of Inorganic Nanostructures in Liquid Phase. *Chem. Rev*. **2014**, 114, 6462–6555.
(34) Palamarciuc, O.; Delahaye, E.; Rabu, P.; Rogez, G. Microwave-assisted post-synthesis modification of layered simple hydroxide. *New J. Chem*. **2014**, 38, 2016
(35) Benito, P.; Labajos, F. M.; Rives, V. Microwaves and layered double hydroxides: A smooth understanding. *Pure Appl. Chem*. **2009**, 81, 1459–1471.
(36) Bovio, B.; Locchi, S. Crystal structure of the orthorhombic basic copper nitrate, $Cu_2(OH)_3NO_3$. *J. Crystallogr. Spectrosc. Res.* **1982**, 16, 507-517
(37) Taviot-Guého,C.; Vialat, P.; Leroux, F.; Razzaghi, F.; Perrot, H.; Sel, O.; Daugaard Jensen, N.; Gro Nielsen, U.; Peulon, S.; Elkaim, E.; Mousty, C. Dynamic Characterization of Inter- and Intralamellar Domains of Cobalt-Based Layered Double Hydroxides upon Electrochemical Oxidation. *Chem. Mater*. **2016**, 28, 7793-7806.
(38) Huang, B.; Wang, W; Pu, T.; Li, J.; Zhu, J. Zhao, C.; Xie, L.; Chen, L.Two-dimensional porous (Co, Ni)-based monometallic hydroxides and bimetallic layered double hydroxides thin sheets with honeycomb-like nanostructure as positive electrode for high-performance hybrid supercapacitors. *J. Colloid Interface Sci*. **2018**, 532, 630-640.
(39) Jacobsen, J.H.; Schnell, S.K. The Importance of Stacking and Coordination for Li, Na, and Mg Diffusion and Intercalation in Ti3C2T2. MXene. *Adv. Mater. Interfaces* **2022**, 9, 2200014
(40) Liu, D.; Shadike, Z.; Lin, R.; Qian, K.; Li, H.; Li, K.; Wang, S.; Yu, Q.; Liu, M.; Ganapathy, S.; Qin, X.; Yang, Q.-H.; Wagemaker, M.; Kang, F.; Yang, X.-Q.; Li, B. Review of Recent Development of In Situ/Operando Characterization Techniques for Lithium Battery Research. *Adv. Mater.* **2019**, 31 1806620.
(41)Fletcher, S.R.; Skapski, A.C. Refined crystal structure of tetra-μ-acetato-bisaquodicopper(II) Patrice de Meester. *J. Chem. Soc., Dalton Trans.* **1973**, 2575-2578.

Electrochemical behavior of morphology controlled copper(II) hydroxide nitrate nanostructures.

Julien Sarmet, Christine Taviot-Gueho,* Rodolphe Thirouard, Fabrice Leroux, Camille Douard, Insaf Gaalich, Thierry Brousse, Gwenaëlle Toussaint and Philippe Stevens

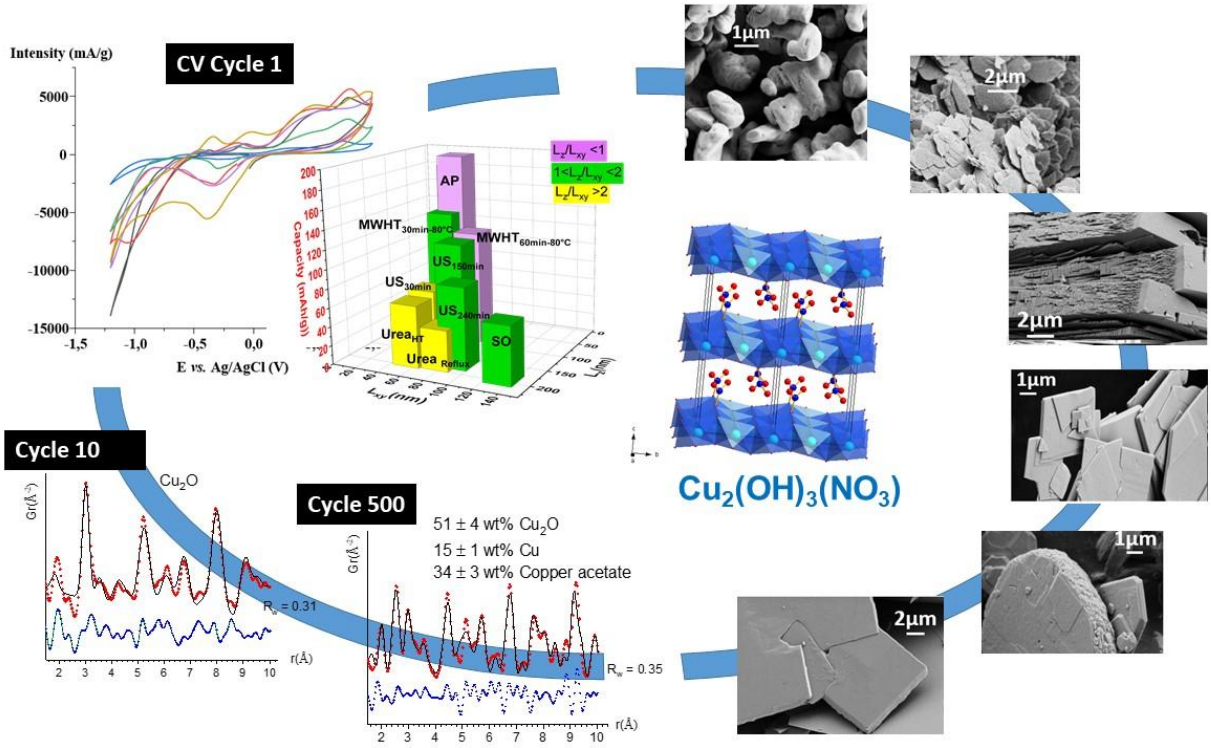

Using different methods of soft chemical synthesis, including microwave and ultrasound methods, it was possible to modulate the nanostructure and particle size of $Cu_2(OH)_3(NO_3)$ LHS, and to observe the effects on the electrochemical capacity and cyclability of that material.